ISSN 1067-8212, Russian Journal of Non-Ferrous Metals, 2016, Vol. 57, No. 5, pp. 445–455. © Allerton Press, Inc., 2016.

PHYSICAL METALLURGY AND HEAT TREATMENT

Effect of Gd on Microstructure, Mechanical Properties and Wear Behavior of As-Cast Mg–5Sn Alloy[1]

Mengqi Cong[a], Ziquan Li[a, b, *], Jinsong Liu[a, c, **], Xuefei Miao[d], Bijun Wang[a], and Qingyang Xi[a]

[a]*College of Materials Science and Technology, Nanjing University of Aeronautics and Astronautics, no. 29 Yudao Street, Nanjing 211100, China*

[b]*Chemical Engineering Department, Nanjing Polytechnic Institute, Nanjing 210048, China*

[c]*State Key Laboratory of Mechanics and Control of Mechanical Structures, Nanjing University of Aeronautics and Astronautics, Nanjing 210016, China*

[d]*Fundamental Aspects of Materials and Energy, Faculty of Applied Science, Delft University of Technology, Mekelweg 15, 2629 JB, Delft, the Netherlands*

**e-mail: ziquanli@nuaa.edu.cn*

***e-mail: jsliu@nuaa.edu.cn*

Received November 17, 2015

Abstract—Effect of minor Gd addition on the microstructure, mechanical properties and wear behavior of as-cast Mg–5Sn-based alloy was investigated by means of OM, XRD, SEM, EDS, a super depth-of-field 3D system, standard high-temperature tensile testing and dry sliding wear testing. Minor Gd addition has strong effect on changing the morphology of the Mg–5Sn binary alloy. Gd addition benefits the grain refinement of the primary α-Mg phase, as well as the formation and homogeneous distribution of the secondary Mg_2Sn phase. The mechanical properties of the Mg–5Sn alloys at ambient and elevated temperatures are significantly enhanced by Gd addition. The wear behavior of the Mg–5Sn alloy is also improved with minor Gd addition. The alloy with 0.8% Gd addition exhibits the best ultimate tensile strength and elongation as well as the optimal wear behavior. Additionally, the worn surface of the Mg–5Sn–Gd becomes smoother in higher Gd-containing alloys. The best wear behavior of alloy was exhibited when Gd addition was up to 0.8%, showing a much smoother worn surface than that of control sample. The improvement of tensile properties is mainly attributed to the refinement of microstructure and the increasing amount and uniform distribution of Mg_2Sn phase. The larger amount of Mg_2Sn phase uniformly distributed at the grain boundary of Mg–Sn–Gd alloys act as a lubrication during sliding, and combined with smaller grain size improve wear behavior of the binary alloy.

Keywords: magnesium alloys, microstructure, mechanical properties, wear behavior

DOI: 10.3103/S1067821216050114

1. INTRODUCTION

Magnesium alloys are widely applied in automotive, aeronautic and astronautic industries, etc., because of their high strength to density ratio, high stiffness to density ratio, as well as environmental protection [1, 2]. Up to now, the most commonly used magnesium alloys are those based on Mg–Al systems. However, the use of these alloys at present is limited by their poor heat-resistance due to the low thermal stability of $Mg_{17}Al_{12}$ phase, especially their creep resistance properties at elevated temperatures (over 408 K) [3, 4]. Consequently, there is a strong demand for the development of heat-resistant magnesium alloys for elevated-temperature applications with acceptable castability and low cost.

The Mg–Sn system has recently received considerable interest [5, 6]. It is an age-hardenable system, which is promising as a cost-effective heat-resistant alloy, since the Mg_2Sn phase (face-centered cubic (FCC), $\alpha_\beta = 0.676$ nm) has a high melting temperature of 1043 K [7, 8]. The dispersed Mg_2Sn precipitations effectively resist deformation and grain boundary sliding in high-temperature environments [9, 10]. Besides, alloying-element Sn also improves the castability and the tensile strength at ambient temperature in Mg-based alloys [11, 12]. However, the Mg–Sn alloys prepared by conventional ingot metallurgy process show very low ductility and strength due to the large particle size of primary α-Mg phase and the large dendrite arm spacing. Therefore, some alloying elements such as rare earth (RE) [13], alkaline-earth elements [14, 15], and Al [16] have been added to Mg–Sn

[1] The article is published in the original.

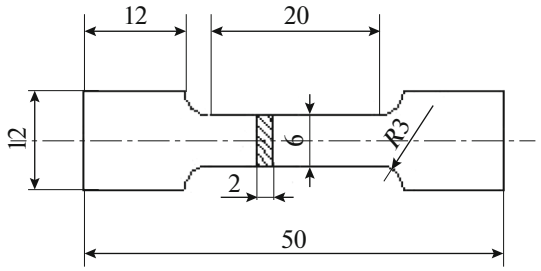

Fig. 1. The shape and size of the samples used for the tensile tests (unit: mm).

system to improve the mechanical properties at ambient and elevated temperatures.

It is well known that the solubility limit of Gd in Mg is relatively higher than those of Ce, Nd, Zr, Sr, Sn and Mn elements in Mg, which may be beneficial to enhance the age-hardening response. In addition, according to the edge-to-edge matching model proposed by Zhang et al., Gd has a grain-refining effect on the Mg alloys [17]. Yamasaki et al. developed warm-extruded Mg–1Zn–2.5Gd (at %) and Mg–2.3Zn–14Gd (wt %) alloys, which exhibit high tensile yield strength (345 MPa) and elongation (6.9%), due to the refinement of the a-Mg grains and the high dispersion of a hard 14H-type long period ordered (LPO) structure phase [18]. As reported by Wang et al., the grain can be refined and thus the thermal resistance is improved in Mg–5Y–3Nd–0.6Zr alloy by Gd addition. The high ultimate tensile strength in Mg–5Y–3Nd–2Gd–0.6Zr alloy has also been mainly attributed to the Gd-induced increase in the α-phase and the Mg_5RE strengthening phase [19]. Microstructure, tensile properties and creep behaviors of as-cast Mg–2Al–1Zn–*x*Gd (x = 1, 2, 3, and 4 wt %) alloys were investigated by Wang et al. They found that the AZ21 alloy containing 4% Gd presents a good creep-resistant property, which is mainly due to the thermal stable branched $(Mg, Al)_3Gd$ phase [20]. Many other studies also indicate that rare earth element Gd is an effective alloying-element for the significant improvement of mechanical properties [21, 22]. Therefore, it is expected that the Gd addition to the Mg–5Sn binary alloy probably also plays a beneficial role in the microstructure, mechanical properties and wear behavior. However, large addition of Gd leads to high cost and inferior plasticity of the alloys and thus will limit their applications. To our knowledge, rare work has been done on the effect of minor Gd-addition on the microstructure, mechanical properties and wear behavior in the Mg–Sn system.

The aim of this paper is to study the effect of minor Gd addition (0, 0.1, 0.3, 0.5, 0.8 and 1.0%) on the microstructure of Mg–5Sn alloy. The influence of minor Gd addition on wear behavior and tensile properties at ambient and elevated (423 K) temperatures is also investigated. It is expected to prepare a new Mg–Sn–Gd alloy with a fine microstructure and the excellent properties.

2. EXPERIMENTAL

Commercial Mg ingot (>99.9%), Sn ingot (>99.8% Nanjing Yanhua Chemical Co., Ltd.) and Mg–45%Gd alloy were used to prepare Mg–5Sn–*x*Gd alloys. The melting process was in an electric resistance furnace under an mixed atmosphere of 1 vol % SF_6 and 99 vol % CO_2. The mixed ingots were first melted at 1043 K for 30 min, then cast into the preheated steel mould (with a size of 100 mm × 80 mm × 20 mm).

For the microstructural observation, the square samples were cut by electric spark machining from the same position in the ingots, then mechanically polished before chemical etching with a 4 vol % nitric alcohol solution. Optical micrographs were taken with a XJP-300 optical microscope using a Canon digital camera. The phase structure were detected and analyzed by a Bruker D8-advance X-ray diffraction (XRD) operated at 40 kV and 40 mA with CuK_α radiation, using a step scan (0.02°/step) of 2θ from 20° to 90° and scanning speed of 1°/min. An energy dispersive X-ray spectrometer (EDS) affiliated with the LEO 1550 scanning electron microscope (SEM) was used for chemical composition analysis.

The tensile samples were prepared from the ingots according to GB/T 228.1-2010 standards [23]. Tensile specimens with a gauge section of 20 mm × 6 mm × 2 mm were performed using a standard high temperature tensile testing machine (SANS-CMT5105) at ambient temperature and at 423 K with a cross-head speed of 0.2 mm/min. The shape and size of the samples used for the tensile tests are shown in Fig. 1. To ensure temperature homogeneity inside the sample, the sample was kept at 423 K for 10 min before starting the tensile test. The tensile properties reported here were an average of five tests and corresponding errors were analyzed.

Dry sliding wear tests without lubricant were conducted using a ball-on-disc type apparatus (HT-500), as illustrated by the schematic layout in Fig. 2. Silicon nitride (Si_3N_4) balls (average hardness of HRC77) with a diameter of 5 mm were used as the counterparts. The material of the disc is commercially available stainless steel sheet. The wear testing specimens with a gauge section of 11 mm × 11 mm × 3 mm were cut by electric spark machining. The contact surfaces were polished by silicon carbide sand paper with fineness up to 1200-grit and ultrasonically cleaned in acetone before putting them in contact with the counter-face. The testing sample was fixed by a fixed plate and

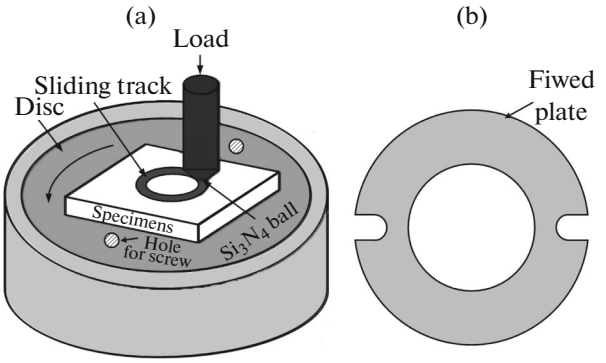

Fig. 2. Schematic representation of ball-on-disc experimental set-up without fixed overlay ring (a) and the fixed overlay ring (b).

screws as shown in Fig. 2b. All tests were performed under ambient temperature using a stationary load of 5 N and a constant sliding speed of 560 rpm for 15 min. The radius of track is 2 mm. Morphologies of the wear surfaces were analyzed by a super depth-of-field 3D system (VHX-1000, Keyence Company) and scanning electron microscope (SEM). The wear resistance was assessed using wear volume loss of the wear specimen after measuring their width and depth of the wear tracks. The following equations were used to calculate wear volume and wear rate of the samples [24]:

$$\Delta V = Sl, \tag{1}$$

$$K = \frac{\Delta V}{PL}, \tag{2}$$

where ΔV is the wear volume (mm^3), S is the cross-sectional area of the wear track (mm^2), which can be measured by corresponding area-measurement function of the super depth-of-field 3D system (VHX-1000), l is the length of the wear track (mm), K is the specific wear rate ($mm^3\ N^{-1}\ m^{-1}$), P is the applied normal load (N) and L is the total path (m).

3. RESULTS AND DISCUSSION

3.1. Microstructure

Figure 3 shows the XRD patterns obtained for Mg–5Sn alloys with different amount of Gd addition. It can be seen that all the Mg–5Sn alloys with or without Gd additions are composed of α-Mg and Mg_2Sn phases. The optical images of as-cast Mg–5Sn alloys with different Gd additions are shown in Fig. 4. It is observed that all the α-Mg phases in the as-cast alloys are dendritic in nature, while the microstruture changes significantly with the addition of Gd. The dendrite arm spacing of the Mg–5Sn binary alloy is relatively large, but the dendrite crystal is broken and thus becomes more uniform with increasing Gd content up to 0.8%. When the Gd addition reaches 1.0%, the dendrite crystal becomes coarser (see Fig. 4f), although it is still smaller than that of binary alloy (see Fig. 4a).

As shown in Fig. 4, the dendrite arm spacing and α-Mg grain size in the Gd-containing alloys are relatively smaller than those in the Mg–5Sn binary alloy. This indicates that the addition of 0.1–1.0% Gd can effectively refine the primary phase of the binary alloy. The grain size of the as-cast Mg–5Sn–*x*Gd alloy decreases first with increasing Gd content up to 0.8% and then slightly increases with increasing Gd addition from 0.8 to 1.0%. The grain size of the as-cast Mg–5%Sn alloy is ~260 μm. When the Gd addition is 0.8%, the grain size reaches ~50 μm, which is the

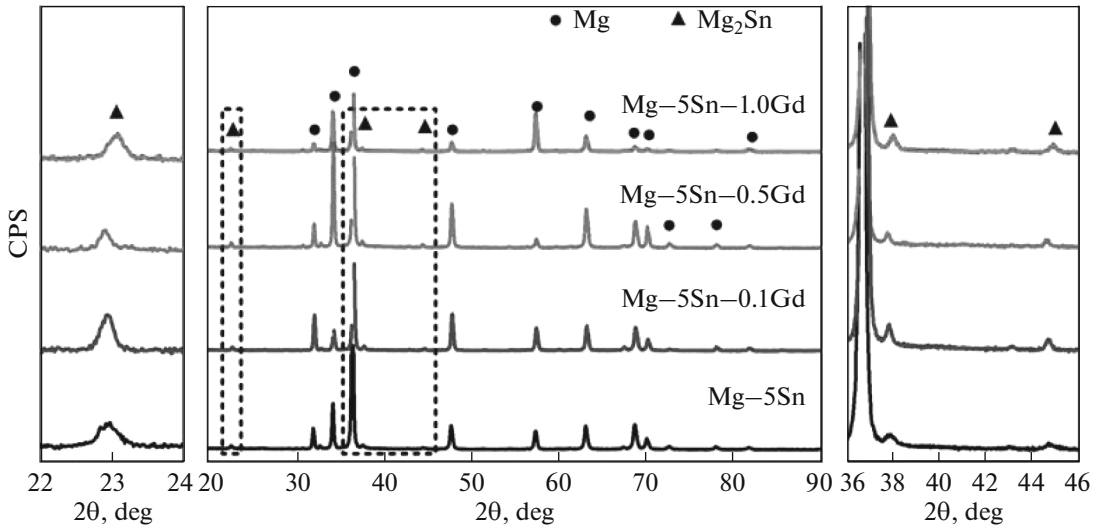

Fig. 3. XRD results of as-cast Mg–5Sn alloys with different Gd additions.

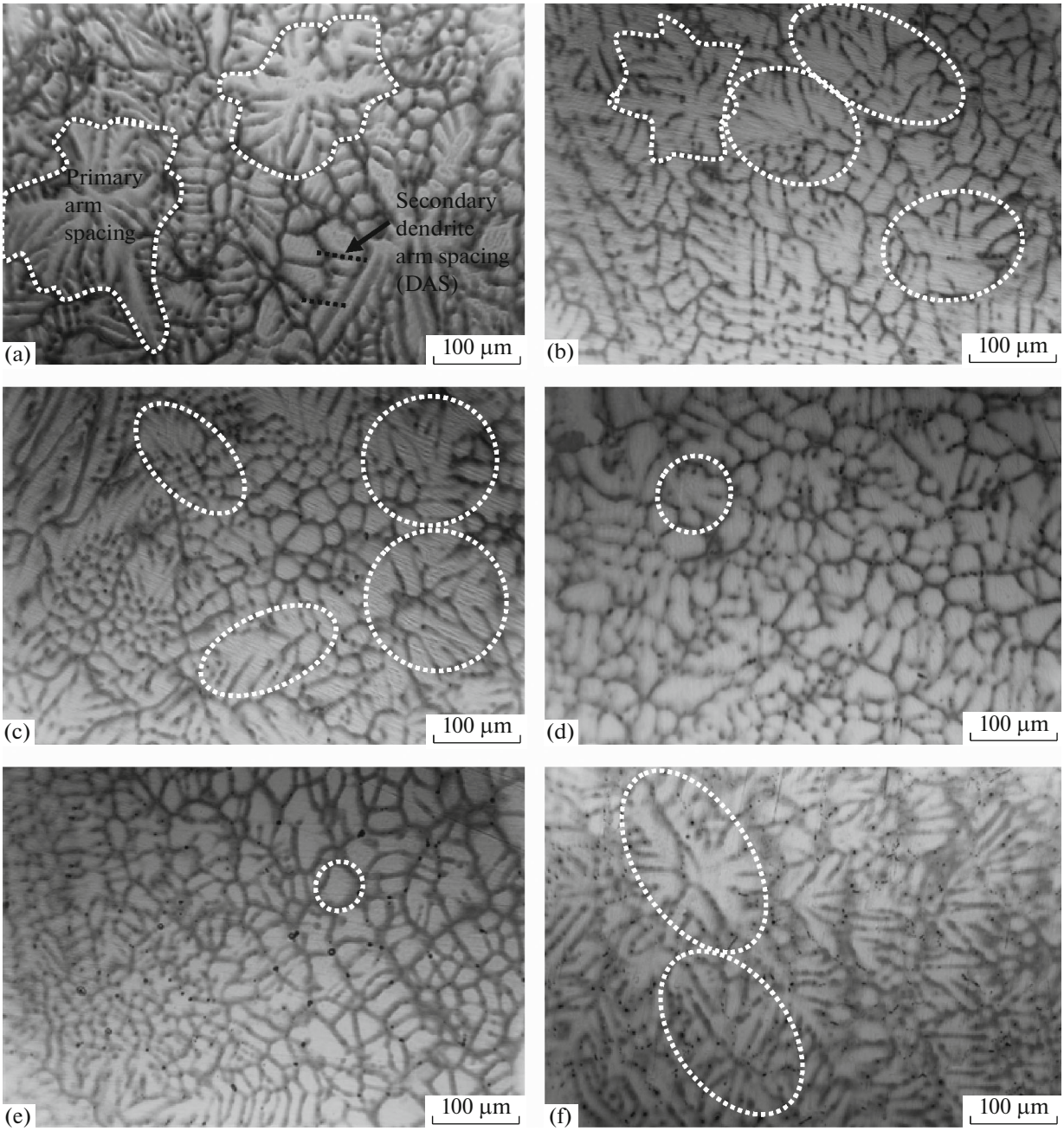

Fig. 4. Optical images of as-cast Mg–5Sn–*x*Gd alloys: (a) 0, (b) 0.1%, (c) 0.3%, (d) 0.5%, (e) 0.8%, (f) 1.0%.

smallest in the experimental alloys. It can be concluded that the most pronounced refinement occurs in the Mg–5Sn–0.8Gd, where the primary dendritic structure is broken and a rather uniform distribution of the microstructure is achieved. Similar refinement effects have been reported after Gd addition to the as-cast Mg–3.8Zn–2.2Ca alloy [25] and Mg–Si alloy [26]. Besides that, the secondary dendritic arm with size of several micrometers could be clearly seen in the Fig. 4. The secondary dendritic spacing also becomes small (shown in Figs. 4a and 4b) and even disappear (shown in Figs. 4c–4f) as the Gd addition increases.

In order to further reveal the microstructure and phase constituent in the magnesium alloys, the SEM images and corresponding EDS analyses for Mg–5Sn and Mg–5Sn–0.5Gd alloys are shown in Fig. 5. It can be clearly seen in Fig. 5a that the intermetallic compound Mg_2Sn was predominately distributed at the grain boundaries and, to a small degree, within the grains. Also, there are some lamellar eutectic structures consist-

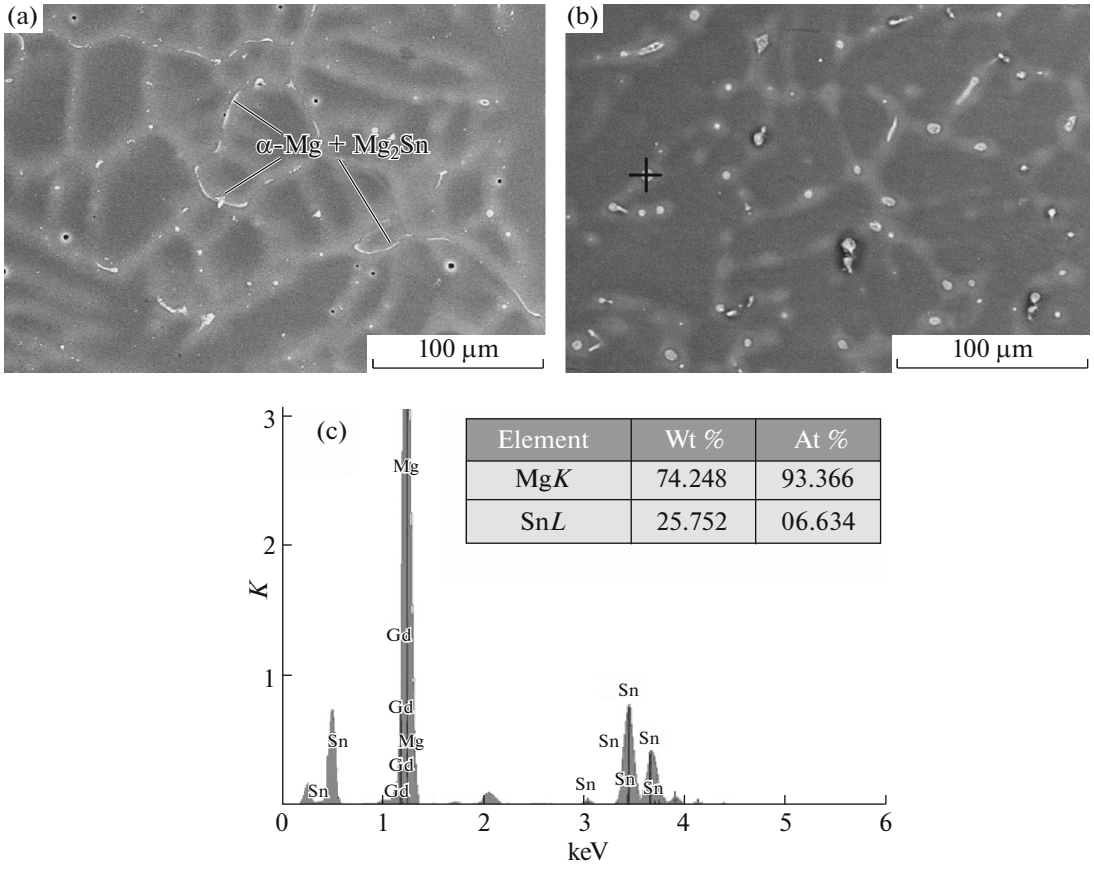

Fig. 5. SEM images of as-cast Mg–5Sn–*x*Gd alloys: (a) 0%, (b) 0.5%, (c) EDS analysis of Mg–5Sn–0.5Gd.

ing of α-Mg and Mg_2Sn at grain boundaries, which is in agreement with the observations from Nayyeri et al. [14]. The Mg_2Sn particle in the Mg–5Sn alloy with 0.5% Gd addition is smaller than that in the binary alloy, and its distribution becomes more uniform (shown in Fig. 5b). Meanwhile, the fine lamellar eutectic structure exhibits short-fiber shape, and the amount of eutectic structures decreases.

It is well known that Gd is a surface active element. And it can easily segregate at the liquid-solid interface or be absorbed in a crystal plane to change the surface energy by lattice distortion. Meanwhile, according to the fundamentals of solidification and the binary Mg–Gd phase diagram, the distribution coefficient of the solute Gd is less than 1 and consequently the solute Gd atoms are enriched in the liquid ahead of the solid-liquid interface during the solidification process [21]. Hence, the growth process are effectively hindered after Gd additions due to the changes of the solid-liquid interfacial energy and the surface energy. As a result, a finer grain of the primary phase is obtained in the Gd-containing alloys. Furthermore, due to the solute redistribution at the solid-liquid interface and the slow diffusion rate of the Gd atom, Gd will lead to the constitutional under-cooling. And the increase of nucleation rate is higher than the grain growth rate, which also leads to the grain refinement. Therefore, it is inferred that microstructure evolution of the Gd-containing alloys is due to the strong growth-restriction effect of the Gd atoms.

3.2. Mechanical Properties

The mechanical properties, including ultimate tensile strength (UTS) and elongation (Elong.), of the Mg–5Sn alloys with different amount of Gd addition at ambient and elevated temperatures are displayed in Fig. 6. It can be found that all of the results are within the accepted error range, and the mechanical properties of the Gd-containing alloys are relatively better than those of the Mg–5Sn binary alloy. This indicates that the addition of Gd to the Mg–5Sn binary alloy can significantly improve the mechanical properties. The ultimate tensile at ambient and elevated tempera-

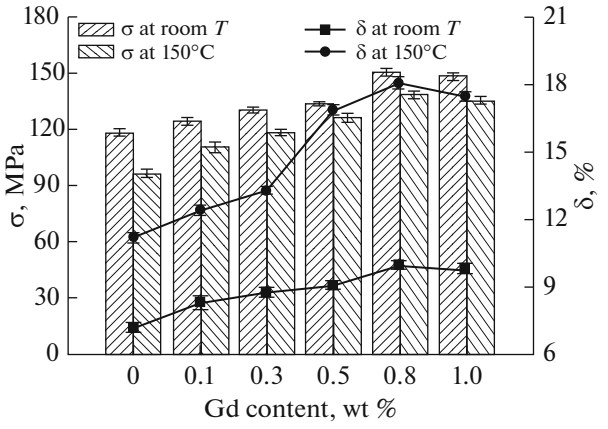

Fig. 6. The mechanical properties of Mg–5Sn–*x*Gd alloys at ambient and elevated temperatures.

tures reaches it maximum at a Gd addition of 0.8%. However, further increase in Gd amount to 1.0% causes a slight reduction in the ultimate tensile strength and elongation.

Fine microstructure is usually beneficial to the mechanical properties of engineering alloys [25]. According to the above description, the dendrite arm spacing and α-Mg grain in the Gd-containing Mg–5Sn alloys are smaller than those in Mg–5Sn binary alloy. Generally, large intermetallic particles favour the initiation and propagation of cracks under applied stress, bringing about a detrimental effect on the tensile strength and ductility [15]. Obviously, the refinement of the primary arm spacing and α-Mg grains is responsible for the improvement of tensile properties. Similarly, the modification of the secondary dendritic spacing also improves the mechanical properties to some extent. In addition, Nayyeri et al. [14] pointed out that Mg_2Sn and CaMgSn particles in Mg–5Sn–*x*Ca alloys mostly lie in the grain boundary region, increasing grain boundary surface. Additionally, the finer and more uniform distribution of these phases through the structure will lead to more stable structure. The larger amount and more uniform distribution of Mg_2Sn phase along the grain boundaries are easier to act as an effective straddle to the dislocation motion, which will improve the tensile properties of Gd-containing Mg–5Sn alloys. Therefore, it can be concluded that the improvement of tensile properties is mainly attributed to two aspects: (1) the refinement of microstructure, mainly through the refinement of lamellar eutectic structures of primary α-Mg phases, and (2) the increasing amount and uniform distribution of the secondary Mg_2Sn phase.

3.3. Wear Resistance

3.3.1. Wear rate. Figure 7 represents a couple (the best and the worse) of experimental 2D track profiles and the cross-sectional areas of the wear track ($\times 10^4$ μm^2). According to the formula (1)–(2), the change trend of

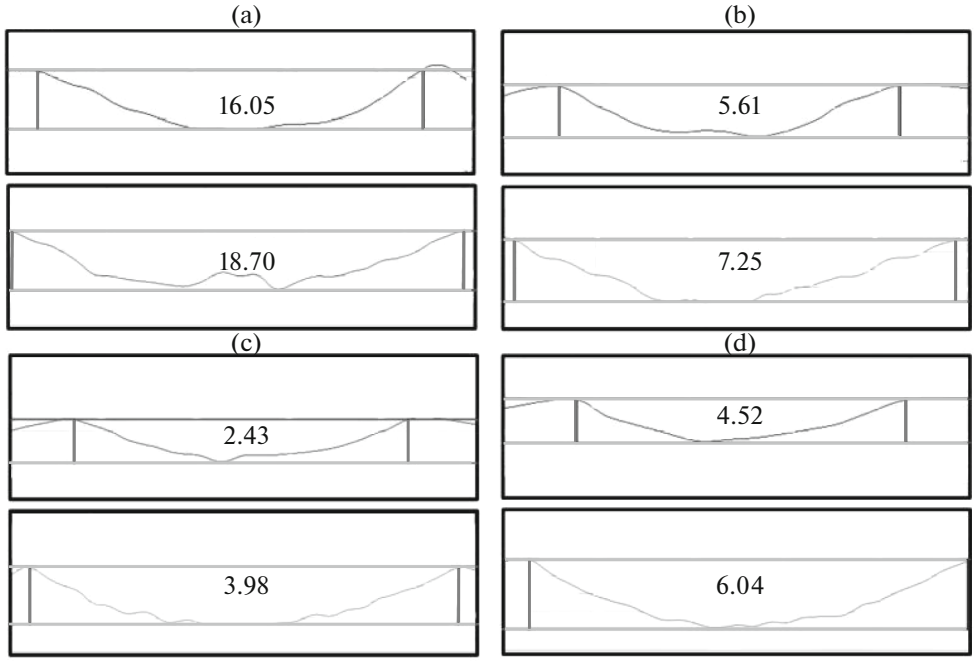

Fig. 7. A couple (the best and the worse) of experimental 2D track profiles and the cross-sectional areas of the wear track: (a) 0, (b) 0.5%, (c) 0.8%, (d) 1.0%.

The wear testing results of the experimental alloys

Sample	Width of wear track, μm	Depth of wear track, μm	Cross-sectional area ($\times 10^{-2}$ mm^2)	Wear rate ($\times 10^{-4}$ mm^3 N^{-1} m^{-1})
Mg–5Sn	1608.62	161.50	17.35	20.65
Mg–5Sn–0.1Gd	1468.85	132.90	10.85	12.91
Mg–5Sn–0.3Gd	1332.73	101.70	8.07	9.60
Mg–5Sn–0.5Gd	1238.75	92.89	6.46	7.68
Mg–5Sn–0.8Gd	986.95	60.02	3.24	3.85
Mg–5Sn–1.0Gd	1153.68	74.77	5.20	6.19

cross-sectional areas in proportion to that of wear rates, which are also calculated and shown in table of the next section. It can be seen that the wear rate decreases with the increase of Gd amount until 0.8%, while it slowly increases as the Gd concentration further increases up to 1.0%. The changing trend of the wear rate is basically coincident with that of mechanical properties. The Mg–5Sn alloy with 0.8% Gd addition shows the lowest wear rate at ambient temperature, indicating the best wear resistance in the Mg–5Sn–0.8Gd alloy.

It is well known that the secondary dendritic spacing is strongly linked to the mechanical properties. The research by Ares et al. has pointed out that a clear inverse relation is observed between the wear resistance and the secondary dendritic spacing, which may explain the increase in wear resistance in the equiaxed region [27, 28].

Consequently, the enhancement of wear resistance by Gd addition is probably due to the changes in the secondary dendritic spacing, which decreases (shown in Figs. 4a, 4b) and even disappear (shown in Figs. 4c–4f) as the Gd addition increases.

3.3.2. Worn surface morphology. Figure 8 represents characteristic scheme of worn behavior for the Mg–5Sn alloys with 0, 0.1, 0.5 and 0.8% Gd additions at ambient temperature. It is found that the worn surfaces exhibit different morphologies, and becomes smoother in the alloys with more Gd addition. Besides that, the worn surface of the experimental alloys is covered with grooves parallel to the sliding direction. The rough traces of parallel grooves can be observed on the worn surface of the binary alloy, as shown in Fig. 8a. There are some fine abrasive joints and debris on the surfaces of the Mg–5Sn–(0.1, 0.5)Gd alloys (shown in Figs. 8b, 8c). This is a typical feature of adhesion and abrasion. In the case of 0.8% Gd addition, the worn surface exhibits the smoothest morphology and finest cracks on plastic deformation flow line. The research by Jiang et al. pointed out that the formation of grooves and cracks on the worn surfaces mainly result from ploughing and cutting of hard particles between the pin and disc [29]. The worn surface becomes smooth under the hydrostatic compressive pressure acting near the asperity contact [30, 31]. These cracks, which are perpendicular to the sliding direction, grow and get interconnected to each other and finally result in the removing of a layer of material to generate a scallops. Such interconnected cracks and craters on the worn surfaces are related to the process of delamination. This is generally known as delamination wear, which is in accordance with the elegant study of Poddar et al. [32].

SEM analysis is excellent for high lateral resolution studies on wear surface, but it is not sensitive to small differences in the z (height) direction because of the large depth of field offered by SEM imaging. Accordingly, a super depth-of-field 3D system was used to investigate the roughness of the wear tracks [33, 34]. Figure 9 shows the 3D morphologies of wear tracks on the surface of the experimental alloys. The wear track results of the experimental alloys, summarized in table, are obtained from the analysis of the 3D morphologies in Fig. 9. It can be found that the width and depth of wear track on the surface of the experimental alloys first decrease with the increase of Gd addition, and reach the minimum at 0.8% Gd addition. The further increase of Gd amount causes an increase in the width and depth of wear track.

There are some white regions observed on the worn surface of Mg–5Sn–0.1Gd alloy. The SEM image and corresponding EDS analysis of the white particle are shown in Fig. 10. The EDS analysis confirms that the white regions mainly consist of Mg and O elements.

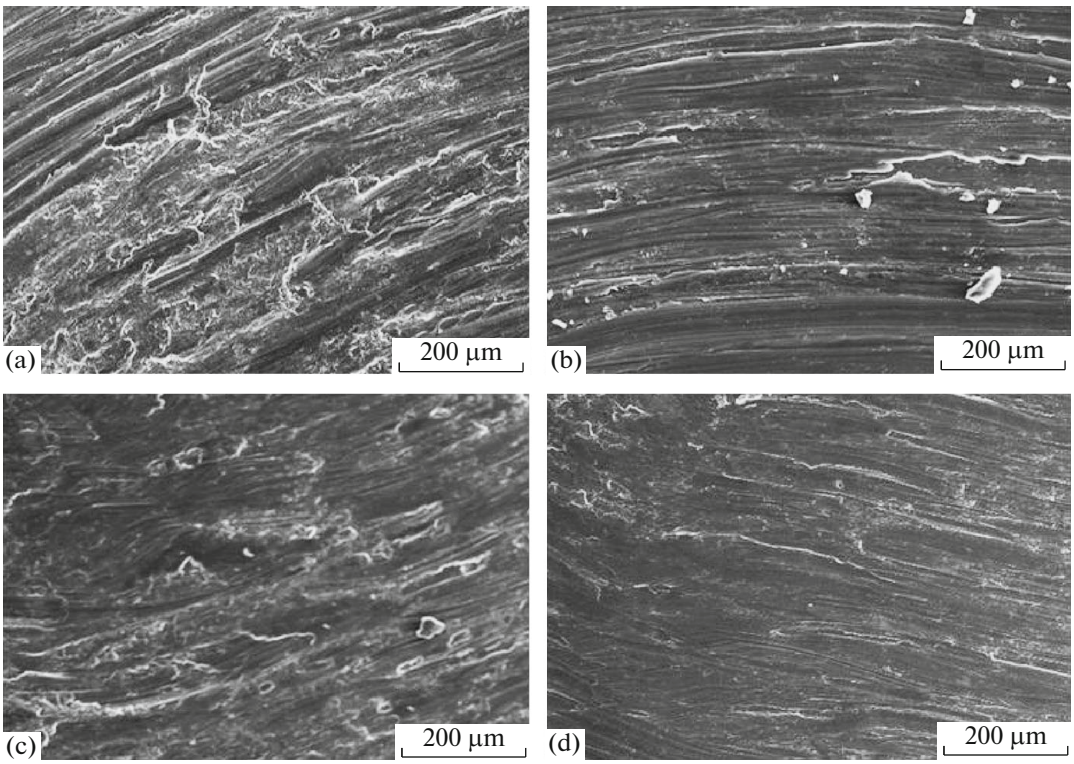

Fig. 8. Characteristic scheme of worn behavior for Mg–5Sn–*x*Gd alloys: (a) 0, (b) 0.1%, (c) 0.5%, (d) 0.8%.

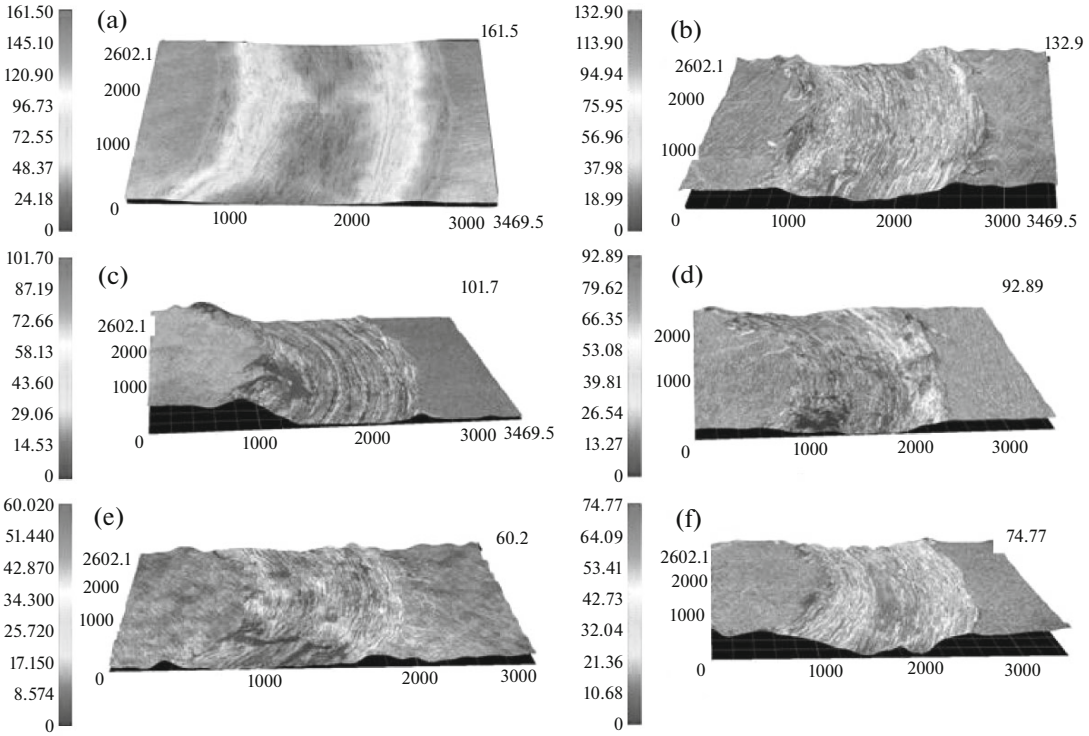

Fig. 9. The 3D morphologies of worn surfaces of Mg–5Sn–*x*Gd alloys at ambient temperature: (a) 0, (b) 0.1%, (c) 0.3%, (d) 0.5%, (e) 0.8%, (f) 1.0%.

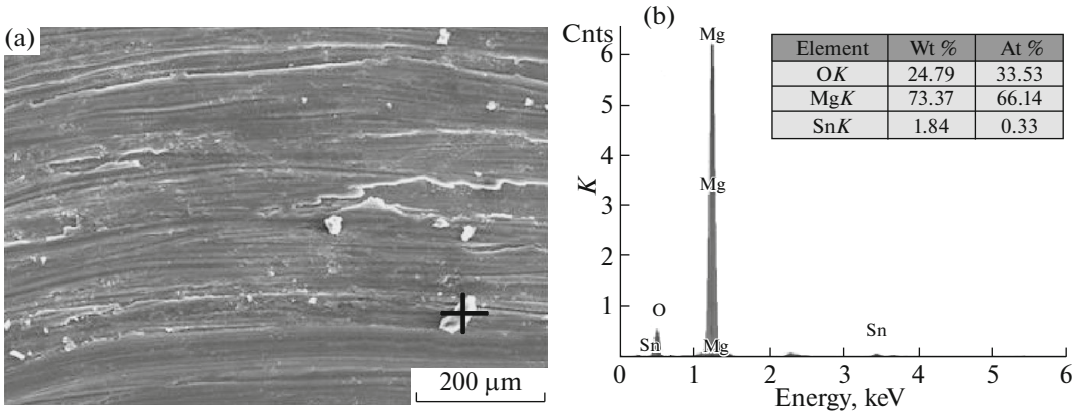

Fig. 10. SEM image (a) and EDS analysis (b) of the white region on the worn surface of Mg–5Sn–0.1Gd alloy.

The research by Yang et al. pointed out that the oxidation of the magnesium matrix appeared at the ambient temperature (298 K) during the wear [35]. Mg easily gets oxidized under ambient conditions, which is mainly attribute to the high chemical activity of Mg element and the low activation energy for the oxidation of Mg ($\Delta G \approx -599$ kJ/mol at 298 K [36]). As a result, the while region on the worn surface of the experimental alloys after the wear test may correspond to MgO. The excess atoms of Mg mainly come from the Mg matrix alloy. It is known that in fretting contacts, oxidation plays a major role in producing the wear damage of metallic materials [37, 38]. Wilson et al. earlier suggested that the tribo-oxides are generally considered to reduce the wear [39]. Yang et al. also pointed out that the oxidation wear is a predominant wear mechanism to keep the wear falling in the mild wear regime due to the oxidation layer containing the oxides of MgO and Fe–Ti–O [35]. During the sliding test, MgO will be peeled off as a particle. With repeated sliding contact, worn surface of the Mg–Sn and Mg–Sn–0.1Gd alloy is dissevered by large MgO particles due to the large size of α-Mg. Small MgO particles in the high Gd-containing alloys fill into the valleys between asperities on the surface and become compacted together. As a result, a layer containing MgO is formed on the sliding surface, which flows easily under shear force and acts as a lubricant during sliding. It has been proposed that the formation of such a surface oxide layer can protect the surface from subsequent wear since the metallic contact is significantly reduced. Obviously, a smaller grain size of the primary phase will lead to a smaller metal oxide size and thus a smaller metallic-contact size. Additionally, compared to the Mg–Sn binary alloy, the larger amount of Mg_2Sn phase uniformly distributed at the grain boundary of Mg–Sn–Gd alloys may also act as a lubrication during sliding. As a consequence, a smoother wear surface is observed in the Mg–Sn–Gd alloys.

4. CONCLUSIONS

The effect of minor Gd addition on the microstructure, mechanical properties and wear behavior of Mg–5Sn alloy has been studied. Minor Gd addition can effectively change the morphology of the Mg–5Sn binary alloy. Gd addition benefits the grain refinement of the primary α-Mg phase, as well as the formation and homogeneous distribution of the secondary Mg_2Sn phase. Due to the modification of the microstructure, the mechanical properties of the Mg–5Sn alloys at ambient and elevated temperatures are enhanced by Gd addition. The alloy with 0.8% Gd addition exhibits the best ultimate tensile strength and elongation. The wear behavior of the Mg–5Sn alloy is significantly improved with minor Gd addition. Optimal wear behavior could be achieved by the Gd addition of 0.8%. Additionally, the worn surface of the Mg–5Sn–Gd becomes smoother in higher Gd-containing alloys. This may be related to the lubrication of Mg_2Sn particles and a surface layer formed on the sliding surface during sliding.

ACKNOWLEDGMENTS

This work was supported by Funding of Jiangsu Innovation Program for Graduate Education (CXZZ13_0160), the Fundamental Research Funds for the Central Universities, Nanjing University of Aeronautics and Astronautics Research Funding (NS2013060), and a Project Funded by the Priority Academic Program Development of Jiangsu Higher Education Institutions.

REFERENCES

1. Razavi, S.M., Foley, D.C., Karaman, I., Hartwig, K.T., Duygulu, O., Kecskes, L.J., Mathaudhu, S.N., and Hammond, V.H., Effect of grain size on prismatic slip in Mg–3Al–1Zn alloy, *Scr. Mater.*, 2012, vol. 67, no. 5, p. 439.
2. Kashefi, N. and Mahmudi, R., The microstructure and impression creep behavior of cast AZ80 magnesium alloy with yttrium additions, *Mater. Des.*, 2012, no. 39, p. 200.
3. Chen, Y.A., Li, J., Yu, S., Liu, H., and Ye, R.Y., Effect of Zn on microstructure and mechanical property of Mg–3Sn–1Al alloys, *Mater. Sci. Eng. A*, 2014, no. 612, p. 96.
4. Shi, Z.Z., The crystallography of lath-shaped Mg_2Sn precipitates in a Mg–Sn–Zn–Mn alloy, *J. Alloys Compd.*, 2013, no. 559, p. 158.
5. Terbush, J.R., Stanford, N., Nie, J.F., and Barnett, M.R., Na partitioning during thermomechanical processing of an Mg–Sn–Zn–Na alloy, *Metall. Mater. Trans. A*, 2013, vol. 44, no. 11, p. 5216.
6. Huang, X.F. and Zhang, W.Z., Characterization and interpretation of interfacial structure of the Mg_2Sn laths in an Mg–Sn–Mn–Ag–Zn alloy, *Philos. Mag. Lett.*, 2014, vol. 94, no. 4, p. 251.
7. Gibson, M.A., Fang, X., Bettles, C.J., and Hutchinson, C.R., The effect of precipitate state on the creep resistance of Mg–Sn alloys, *Scr. Mater.*, 2010, vol. 63, no. 8, p. 899.
8. Poddar, P., Das, A., and Sahoo, K.L., Dry sliding wear characteristics of gravity die-cast magnesium alloys, *Metall. Mater. Trans. A*, 2014, vol. 45, no. 4, p. 2270.
9. Kang, D.H., Park, S.S., and Kim, N.J., Development of creep resistant die cast Mg–Sn–Al–Si alloy, *Mater. Sci. Eng. A*, 2005, vol. 413–414, p. 555.
10. Liu, H., Chen, Y., Tang, Y., Wei, S., and Niu, G., The microstructure, tensile properties and creep behavior of as-cast Mg–(1–10)%Sn alloys, *J. Alloys Compd.*, 2007, vol. 440, no. 1–2, p. 122.
11. Park, S.S., Kim, Y.J., Cheng, W.L., Kim, Y.M., and You, B.S., Tensile properties of extruded Mg–8Sn–1Zn alloys subjected to different heat treatments, *Phil. Mag. Lett.*, 2011, vol. 91, no. 1, p. 37.
12. Ha, H.Y., Kang, J.Y., Kim, S.G., Kim, B., Park, S.S., Yim, C.D., and You, B.S., Influences of metallurgical factors on the corrosion behaviour of extruded binary Mg–Sn alloys, *Corr. Sci.*, 2014, vol. 82, no. 2, p. 369.
13. Wang, Q., Chen, Y.G., Xiao, S.F., Zhang, X.P., Tang, Y.B., Wei, S.H., and Zhao, Y.H., Study on microstructure and mechanical properties of as-cast Mg–Sn–Nd alloys, *J. Rare Earths*, 2010, vol. 28, no. 5, p. 790.
14. Nayyeri, G. and Mahmudi, R., Effects of Ca additions on the microstructural stability and mechanical properties of Mg–5% Sn alloy, *Mater. Des.*, 2011, vol. 32, no. 3, p. 1571.
15. Liu, H.M., Chen, Y.G., Zhao, H.F., Wei, S.H., and Gao, W., Effects of strontium on microstructure and mechanical properties of as-cast Mg–5wt % Sn alloy, *J. Alloys Compd.*, 2010, vol. 504, no. 2, p. 345.
16. Elsayed, F.R., Sasaki, T.T., Mendis, C.L., Ohkubo, T., and Hono, K., Compositional optimization of Mg–Sn–Al alloys for higher age hardening response, *Mater. Sci. Eng. A*, 2013, no. 566, p. 22.
17. Zhang, M.X., Kelly, P.M., Qian, M., and Taylor, J.A., Crystallography of grain refinement in Mg–Al based alloys, *Acta Mater.*, 2005, vol. 53, no. 11, p. 3261.
18. Yamasaki, M., Anan, T., Yoshimoto, S., and Kawamura, Y., Mechanical properties of warm-extruded Mg–Zn–Gd alloy with coherent 14H long periodic stacking ordered structure precipitate, *Scr. Mater.*, 2005, vol. 53, no. 7, p. 799.
19. Wang, L.D., Xing, C.Y., Hou, X.L., Wu, Y.M., Sun, J.F., and Wang, L.M., Microstructures and mechanical properties of as-cast Mg–5Y–3Nd–Zr–xGd (x = 0, 2 and 4 wt %) alloys, *Mater. Sci. Eng. A*, 2010, vol. 527, nos. 7–8, p. 1891.
20. Wang, X.D., Du, W.B., Liu, K., Wang, Z.H., and Li, S.B., Microstructure, tensile properties and creep behaviors of as-cast Mg–2Al–1Zn–xGd (x = 1, 2, 3, and 4 wt %) alloys, *J. Alloys Compd.*, 2012, no. 522, p. 78.
21. Yu, H.Y., Yan, H.G., Chen, J.H., Su, B., Zheng, Y., Shen, Y.J., and Ma, Z.J., Effects of minor Gd addition on microstructures and mechanical properties of the high strain-rate rolled Mg–Zn–Zr alloys, *J. Alloys Compd.*, 2014, no. 586, p. 757.
22. Yang, J., Xiao, W.L., Wang, L.D., Wu, Y.M., Wang, L.M., and Zhang, H.J., Influences of Gd on the microstructure and strength of Mg–4.5Zn alloy, *Mater. Charact.*, 2008, vol. 59, no. 11, p. 1667.
23. National Standard of the People's Republic of China-GB/T *228.1–2010: Metallic Materials-Tensile Testing, Part 1: Method of Test at Room Temperature*, Beijing: China Standard Press, 2011 [in Chinese].
24. Petrzhik, M.I. and Levashov, E.A., Modern methods for investigating functional surfaces of advanced materials by mechanical contact testing, *Crystallogr. Rep.*, 2007, vol. 52, no. 6, p. 966.
25. Yang, M.B., Guo, T.Z., and Li, H.L., Effects of Gd addition on as-cast microstructure, tensile and creep properties of Mg–3.8Zn–2.2Ca (wt %) magnesium alloy, *Mater. Sci. Eng. A*, 2013, no. 587, p. 132.
26. Ye, L.Y., Hu, J., Tang, C.P., Zhang, X.M., Deng, Y.L., Liu, Z.Y., and Zhou, Z.L., Modification of Mg_2Si in Mg–Si alloys with gadolinium, *Mater. Charact.*, 2013, no. 79, p. 1.
27. Ares, A.E., Gassa, L.M., Schvezov, C.E., and Rosenberger, M.R., Corrosion and wear resistance of hypoeutectic Zn–Al alloys as a function of structural features, *Mater. Chem. Phys.*, 2012, vol. 136, nos. 2–3, p. 394.
28. Rosenberger, M.R., Ares, A.E., Gatti, I.P., and Schvezov, C.E., Wear resistance of dilute Zn–Al alloys, *Wear*, 2010, vol. 268, no. 11, p. 1533.
29. Jiang, J., Bi, G.L., Zhao, L., Li, R.G., Lian, J.S., and Jiang, Z.H., Dry sliding wear behavior of extruded Mg–Sn–Yb alloy, *J. Rare Earth*, 2015, no. 33, p. 77.
30. Jahanmir, S. and Suh, N.P., Mechanics of subsurface void nucleation in delamination wear, *Wear*, 1977, vol. 44, no. 1, p. 17.

31. Anbu Selvan, S. and Ramanathan, S., Dry sliding wear behavior of as-cast ZE41A magnesium alloy, *Mater. Des.*, 2010, vol. 31, no. 4, p. 1930.

32. Poddar, P., Das, A., and Sahoo, K.L., Dry sliding wear characteristics of rheocast Mg–Sn based alloys, *Mater. Des.*, 2014, no. 54, p. 820.

33. Xu, Y., Miao, Q., Liang, W.P., Yu, X.S., Jiang, Q., Zhang, Z.G., Ren, B.L., and Yao, Z.J., Tribological behavior of Al_2O_3/Al composite coating on γ-TiAl at elevated temperature, *Mater. Charact.*, 2015, no. 101, p. 122.

34. Walker, J.C., Ross, I.M., Reinhard, C., Rainforth, W.M., and Hovsepian, P.E., High temperature tribological performance of CrAlYN/CrN nanoscale multilayer coatings deposited on gamma-TiAl, *Wear*, 2009, vol. 267, nos. 5–8, p. 965.

35. Yang, Z.R., Wang, S.Q., Zhao, Y.T., and Wei, M.X., Evaluation of wear characteristics of Al_3Tip/Mg composite, *Mater. Charact.*, 2010, vol. 61, no. 5, p. 554.

36. Chase, M.W., NIST-JANAF thermochemical tables, *J. Phys. Chem. Ref. Data, MoNo.gr*, 1998, no. 9, p. 1.

37. Waterhouse, R.B., Fretting wear, *Wear*, 1984, vol. 100, nos. 1–3, p. 107.

38. Manoj Kumar, B.V., Basu, B., Murthy, V.S.R., and Gupta, M., The role of tribochemistry on fretting wear of Mg–SiC particulate composites, *Compos., Part A*, 2005, vol. 36, no. 1, p. 13.

39. Wilson, S. and Alpas, A.T., Thermal effects on mild wear transitions in dry sliding of an aluminum alloy, *Wear*, 1999, nos. 225–229, p. 440.